The semiconductor-metal transition in fluid selenium: an *ab initio* molecular-dynamics simulation

1998 J. Phys.: Condens. Matter 10 1199

(http://iopscience.iop.org/0953-8984/10/6/003)

J. Phys.: Condens. Matter **10** (1998) 1199–1210. Printed in the UK PII: S0953-8984(98)88036-3

The semiconductor–metal transition in fluid selenium: an *ab initio* molecular-dynamics simulation

Fuyuki Shimojo†, Kozo Hoshino†, Mitsuo Watabe† and Y Zempo‡

† Faculty of Integrated Arts and Sciences, Hiroshima University, Higashi-Hiroshima 739, Japan
‡ Sumitomo Chemical, 6 Kitahara, Tsukuba 300-32, Japan

Received 1 October 1997

Abstract. The semiconductor–metal transition in fluid selenium is investigated by means of an *ab initio* molecular-dynamics simulation using the generalized-gradient-corrected density functional theory. It is found that the chain-like structure persists even in the metallic state, although the chain structure is substantially disrupted. The average chain length decreases with increasing temperature, in agreement with the experimentally observed tendency. The detailed investigation of the time change of the chain structure shows that the interaction between the Se chains is crucially important for bond breaking, and that bond breaking and rearrangement of the Se chains occur more frequently at higher temperatures. It is important to note that when the Se–Se bonds break, the anti-bonding states above the Fermi level (E_F) are stabilized while the bonding or non-bonding states below the E_F become unstable, and, therefore, the gap at E_F disappears at high temperatures.

1. Introduction

Crystalline Se has a trigonal structure, consisting of hexagonal arrays of helical chains of atoms with twofold coordination. It shows semiconducting properties, and its electronic structure and the nature of its bonding have been well clarified by various experimental and theoretical studies [1]. The electronic density of states below the Fermi level (E_F) separates basically into three states: s-like states which lie in the low-energy region, p-like bonding states, and p-like non-bonding states, while the electronic states above E_F correspond to p-like anti-bonding states.

The chain structure with twofold coordination is preserved on melting. Near the melting point, liquid Se exhibits semiconducting behaviour similar to that of crystalline Se, and the average chain length has been estimated to be about 10^5 atoms [2, 3]. With increases in the temperature and pressure, the average chain length decreases rapidly, and approaches a length of only about ten atoms near the critical point [4]. Accompanying this structural change, there is an increase in the electrical conductivity [5, 6]. It is interesting to note that, as shown in figure 1, a metallic state, whose conductivity approaches several hundreds of Ω^{-1} cm^{-1}, appears on application of relatively modest pressures, $\geqslant$1 kbar, near the critical temperature.

Edeling and Freyland [7] investigated for the first time the static structure of liquid Se over a wide range of temperatures up to 1400 °C at pressures above the corresponding saturation pressure by means of neutron diffraction, though the temperature and pressure range for which measurements were made is far from the supercritical region in which the metallic state appears. They concluded from an analysis of the pair distribution function that

0953-8984/98/061199+12$19.50

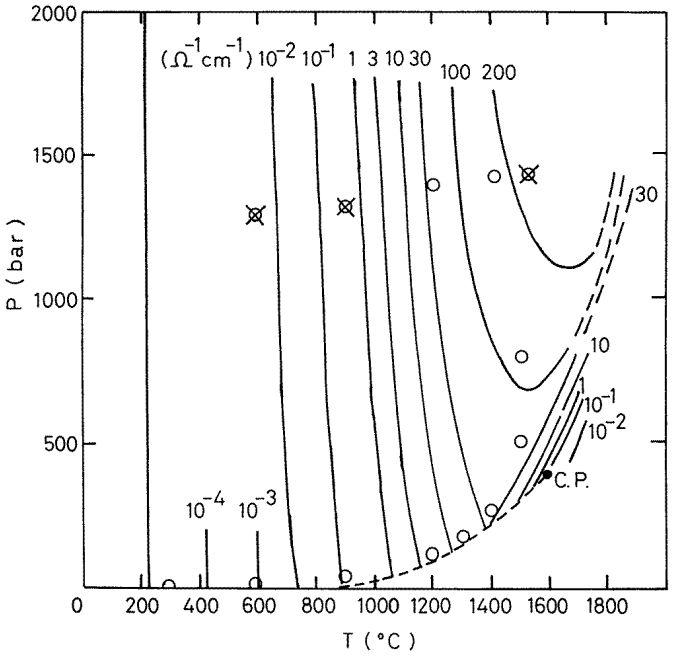

Figure 1. The pressure–temperature phase diagram with the contours of constant dc conductivity in liquid and supercritical fluid Se [5, 6]. The open circles show the temperatures and the pressures for which the x-ray diffraction studies were carried out by Tamura and collaborators [8–10]. Our MD simulations are carried out for three thermodynamic states shown by crosses. The dashed line shows the liquid–vapour coexistence curve. The longer-dashed lines show the extrapolation of the constant dc conductivity curves, where no experimental measurement has been made.

the twofold-coordinated chain structure persists near the critical point. Recently, Tamura and collaborators [8–10] carried out x-ray diffraction measurements for fluid Se up to the supercritical region, including the semiconductor–metal (SC–M) transition region. It was found that the twofold-coordinated structure is largely preserved even in the metallic region, and that the nearest-neighbour distance decreases slightly when the SC–M transition occurs.

The SC–M transition in fluid Se has the following two characteristic features [9]: (1) the electrical conductivity increases with volume expansion; and (2) the metallic states appear when the average chain length becomes very short, which indicates that the SC–M transition correlates with the instability of the chain structure [4, 9, 11]. However, the microscopic mechanism of the SC–M transition has not yet been clarified.

On the other hand, there have been several theoretical studies for liquid Se [12–16] as well as for crystalline trigonal Se [17–19], amorphous Se [20, 21], Se clusters [22], and isolated helical chains [23, 24]. Hohl and Jones [12] carried out *ab initio* molecular-dynamics (MD) simulations for liquid and amorphous Se over the temperature range 350–720 K. They used 64 Se atoms, and the total energy was calculated using the density functional formalism with a local-density approximation (LDA) for the exchange–correlation energy. They examined the static and dynamic properties, including pair distribution functions, bond-angle and dihedral-angle distribution functions, phonon densities of states, and diffusion constants, and then compared them with the experimental results. Bichara *et al* [14] also investigated the structure of liquid and amorphous Se by means of a Monte Carlo

(MC) simulation using the semiempirical model based on a tight-binding approximation of the cohesive energy. They utilized a fairly large system including 648 Se atoms. They showed that the calculated structures are in good agreement with the experiments, and asserted that liquid Se consists of rather short branched chains, even near the melting point, contrary to commonly reported ideas, such as those stated above. More recently, Kirchhoff *et al* [16] carried out *ab initio* MD simulations based on the density functional theory to study liquid Se at three temperatures; 570, 870, and 1370 K along the liquid–vapour coexistence curve. They utilized a system of 69 Se atoms. They showed that the pair distribution functions obtained using the generalized gradient approximation for the exchange–correlation energy are in much better agreement with the experimental results than those obtained using the LDA, especially in the region of the first minimum. In their calculations, the fraction of twofold-coordinated atoms is almost 100% near the melting point. This is in agreement with the experimental measurements, and is different from the result obtained using the tight-binding approximation of Bichara *et al*: 70% [14]. It was found, however, that, at 1370 K, the numbers of onefold- and threefold-coordinated atoms increase, and so the simple chain-like structure is considerably disrupted.

In this paper, we report the results of an *ab initio* MD simulation of the SC–M transition in fluid Se. To our knowledge, no other *ab initio* MD simulations have been carried out to investigate the metallic state of fluid Se. The purposes of our MD simulation are:

(i) to clarify how the structure of fluid Se changes when the SC–M transition occurs;

(ii) to compare the structural changes obtained from our simulation with experiment [8–10]; and

(iii) to investigate the microscopic mechanism of the SC–M transition.

The method of calculation is described briefly in section 2. The results of our simulation and a discussion are given in section 3. Finally section 4 summarizes our work.

2. The method of calculation

Our calculations are performed within the framework of the density functional theory. The generalized gradient approximation [25] is used for the exchange–correlation energy. The electronic wavefunctions are expanded in the plane-wave (PW) basis set. The energy functional is minimized using an iterative scheme based on the preconditioned conjugate-gradient method [26–28]. For the interaction between the valence and core electrons, we used the ultrasoft pseudopotential proposed by Vanderbilt [29].

The cubic supercell contains 81 Se atoms with periodic boundary conditions. Three simulations are carried out at different temperatures and densities: (870 K, 0.0286 Å^{-3}), (1170 K, 0.0270 Å^{-3}), and (1770 K, 0.0254 Å^{-3}), which are indicated in figure 1 by crosses. These densities correspond to the supercell sizes $L = 14.15$, 14.42, and 14.72 Å, respectively, with L being a side of the supercell. These states are selected because x-ray diffraction measurements [9, 10] have been carried out under the same conditions. The states at two temperatures, 870 and 1170 K, are in the semiconducting region, while the state at 1770 K is in the metallic region. The size of the system would be a problem for simulating the states just above the melting point, because the Se chains contain about 10^5 atoms. However, it would be adequate to reproduce the states at higher temperatures, especially near the critical point, where the average number of atoms per chain is only ten. As shown in the following sections, we have succeeded in reproducing the SC–M transition using a system of 81 Se atoms.

Using the Nosé–Hoover thermostat technique [30, 31], the equations of motion are

solved via the velocity Verlet algorithm with time steps $\Delta t = 3.12$, 2.64, and 2.16 fs for the states at 870, 1170, and 1770 K, respectively. The Γ point alone is used to sample the Brillouin zone of the supercell, and the wavefunctions are expanded in the PW basis with a cut-off energy of 11 Ryd. The initial charge density at each MD step is estimated by extrapolating the charge densities at the previous steps [27], and the initial wavefunctions are estimated from the wavefunctions at the previous steps by means of a subspace diagonalization [32]. Each simulation is carried out for at least 4.5 ps. The quantities of interest are obtained by averaging over about 3 ps after the initial equilibration taking about 1.5 ps.

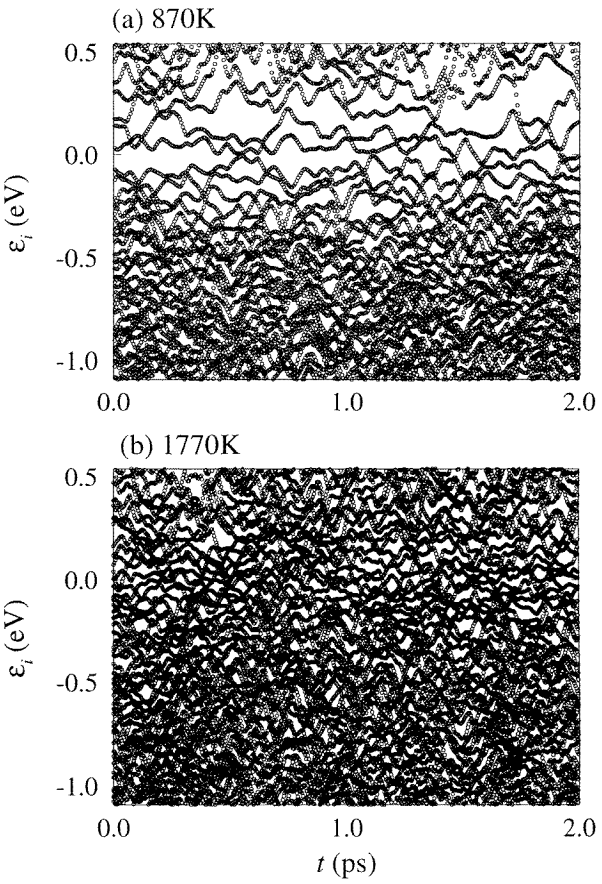

Figure 2. The time evolution of the single-electron eigenvalues ε_i for two temperatures, (a) 870 K and (b) 1770 K. The origin of energy ($\varepsilon_i = 0$) is taken to be the Fermi level.

3. Results and discussion

3.1. The electronic density of states

In figure 2, we show the time evolution of the single-electron eigenvalues ε_i near the Fermi level ($E_F = 0$) obtained from our MD simulations for two temperatures, 870 and 1770 K. It is seen from this figure that, at 870 K, there are few states in the energy range

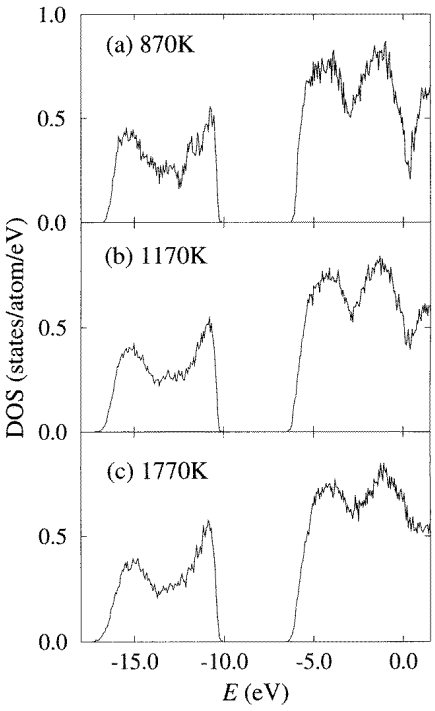

Figure 3. Electronic densities of states of fluid Se for temperatures of (a) 870 K, (b) 1170 K, and (c) 1770 K. The origin of energy ($E = 0$) is taken to be the Fermi level.

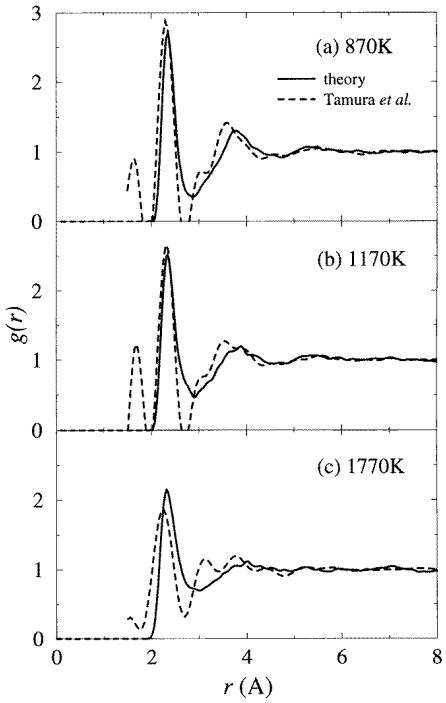

Figure 4. Pair distribution functions $g(r)$ of fluid Se calculated at temperatures of (a) 870 K, (b) 1170 K, and (c) 1770 K, compared with the experimental results [9, 10]. The solid and dashed lines show the calculated and experimental results, respectively.

of $\sim$0.5 eV around the E_F, which means that a semiconductor-like state is reproduced. Since the temperature 870 K is rather high compared with the melting temperature, the chain structure is fairly disrupted. Therefore, we cannot see a clear gap near E_F. On the other hand, at 1770 K, the eigenvalues distribute densely below and above E_F as shown in figure 2(b), which indicates a metallic state. Figure 3 shows the temperature dependence of the electronic density of states (DOS) in fluid Se, which is obtained from a time average of the distribution of the single-electron eigenvalues shown in figure 2. We have also calculated the DOS with multiple k-points in the Brillouin zone of the supercell for some atomic configurations, and the results are almost the same as those shown in figure 3. We see from figure 3 that the electronic structure of fluid Se up to 1170 K is similar to that of trigonal Se, even though the temperatures are relatively high. The electronic states between -17 and -10 eV are s-like in character, those between -7 and -3 eV show p-like bonding, those between -3 and 0 eV show p-like non-bonding, and those above 0 eV show p-like anti-bonding. There is a dip at E_F in the DOS instead of a gap, because of taking the time average. We can, however, see a gap when the DOS is calculated at a fixed atomic configuration. In this case, the width and the position of the gap depend on the time as shown in figure 2. On the other hand, at 1770 K, the dip at E_F disappears, and there is no distinction between the p-like non-bonding and the p-like anti-bonding states. Thus, we have succeeded in reproducing the SC–M transition in fluid Se with our *ab initio* MD simulations.

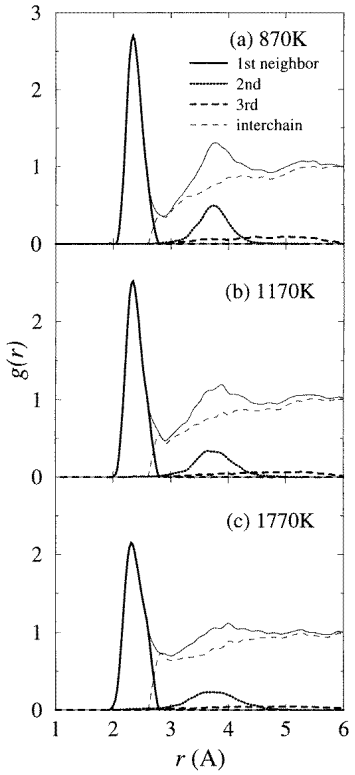

Figure 5. Interchain and intrachain pair distribution functions of fluid Se calculated at (a) 870 K, (b) 1170 K, and (c) 1770 K. The bold solid, the bold dotted, and the bold dashed lines show the first-neighbour, the second-neighbour, and the third-neighbour intrachain pair distribution functions, respectively. The thin dashed line shows the interchain pair distribution function, and the thin solid line shows the total $g(r)$ as shown in figure 4.

3.2. Pair distribution functions

To examine how structural changes occur with the SC–M transition in fluid Se, and to compare them with the experimental data of Tamura and collaborators [9, 10], we calculate the pair distribution functions (PDF) $g(r)$, and show them in figure 4 for three temperatures, 870, 1170, and 1770 K. The solid and dashed lines show the calculated and experimental results, respectively. From this figure, we can see that the calculated results are in reasonable agreement with the experimental results, though some deviations between them are recognized. Since the x-ray diffraction measurements of Tamura *et al* were performed under very difficult conditions, it is very hard to obtain the static structure factors $S(k)$ precisely for the wide range of k-vectors. The experimental $S(k)$ data in the large-k region are rather scattered, which causes a truncation error in the Fourier transform of $S(k)$; that is, the peaks at around $r = 1.6$ Å shown in figures 4(a) and 4(b) have no physical meaning, and the data below $k = 1$ Å^{-1} are obtained by interpolation to the $S(0)$ value estimated from the thermodynamic values. It is, therefore, expected that the $g(r)$ derived from the experimental $S(k)$ has some ambiguities. Considering these facts, we conclude that the differences between the calculated and experimental results are not important, and that we have succeeded in reproducing the structure of fluid Se over a wide range of temperatures.

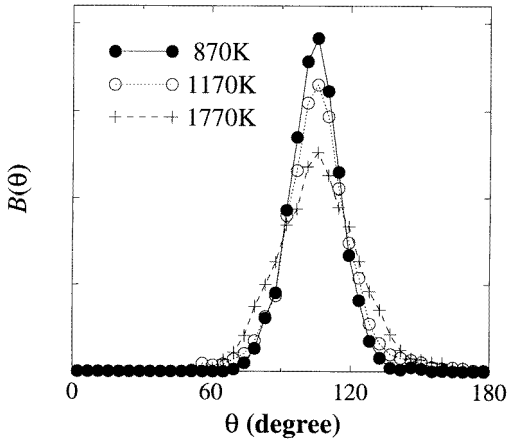

Figure 6. Bond-angle distribution functions $B(\theta)$ for fluid Se calculated at 870 K (solid line with solid circles), 1170 K (dotted line with open circles), and 1770 K (dashed line with plus symbols).

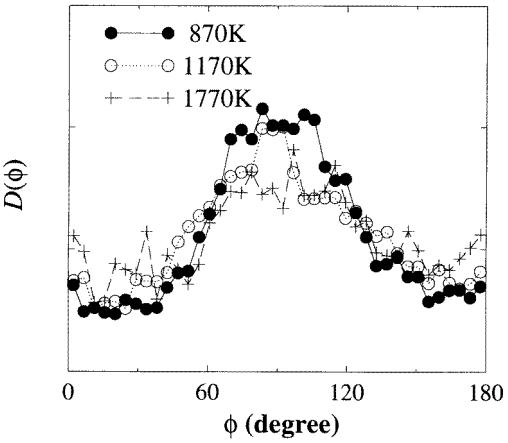

Figure 7. Dihedral-angle distribution functions $D(\phi)$ for fluid Se calculated at 870 K (solid line with solid circles), 1170 K (dotted line with open circles), and 1770 K (dashed line with plus symbols).

It is seen from figure 4 that the first peak of $g(r)$ is sharp, even at 1770 K, which means that the chain-like structure remains in the metallic state. However, the first peak becomes lower and the first minimum becomes shallower with increasing temperature, which means that the chain structure is more disrupted at higher temperatures. The position r_1 of the first peak of $g(r)$ moves slightly to smaller r. The values of r_1 are 2.35, 2.34, and 2.32 Å at 870, 1170, and 1770 K, respectively. It should be noted that these average nearest-neighbour distances are a little smaller than the distance found for trigonal Se: 2.37 Å. The coordination number N_1, which is here estimated by the formula $2\rho\int_0^{r_1} 4\pi r^2 g(r)\,\mathrm{d}r$, where ρ is the number density of atoms, decreases slightly, which means that the average chain length decreases as the temperature increases. The values of N_1 are 1.9, 1.7, and 1.5 at 870, 1170, and 1770 K, respectively. Though there are different definitions for the coordination

number which give slightly different results quantitatively, the qualitative features do not change.

To investigate in more detail how the chain structure changes with increases in the temperature, let us try to decompose the system into an assembly of twofold-coordinated chains. In order to do this, we decide whether the two Se atoms belong to the same chain or not simply by considering the distance between them. If the distance between the two Se atoms is smaller than 2.7 Å, the position of the first minimum of $g(r)$, we consider that they belong to the same chain, and otherwise that they do not. In figure 5, we show the first-neighbour (bold solid line), the second-neighbour (bold dotted line), and the third-neighbour (bold dashed line) intrachain PDFs as well as the interchain PDF (thin dashed line). It is found that the second-neighbour intrachain PDF together with the interchain PDF contribute to form the second peak of $g(r)$, and the second peak becomes broader with increasing temperature. The third-neighbour intrachain PDF is very broad at any temperature. The first minimum of $g(r)$ is determined mainly by the interchain PDF, and becomes shallow at 1770 K. For these reasons the first minimum of $g(r)$ can be considered as the measure of how much the chain structure is disrupted. Note that the first minimum of $g(r)$ is zero and the first peak is separated from the second peak for the liquid Se near the melting temperature, where the liquid Se is composed of many long chains with about 10^5 atoms each.

3.3. Bond-angle and dihedral-angle distribution functions

Figures 6 and 7 show the bond-angle (θ) distribution function $B(\theta)$ and the dihedral-angle (ϕ) distribution function $D(\phi)$, respectively. As shown in figure 6, $B(\theta)$ at each temperature has a peak at 105°, which is almost the same as or slightly larger than the value for trigonal Se, 103°. It is found that the peak of $B(\theta)$ becomes lower and broader with increasing temperature. Compared with $B(\theta)$, $D(\phi)$ has a broad distribution as shown in figure 7. It is seen that $D(\phi)$ has no peak but has a plateau in the range from $\phi = 70°$ to 110°, which should be compared with the dihedral angle of trigonal Se (101°) and that of an isolated helical Se chain (75°). In the metallic state, i.e. at 1770 K, $D(\phi)$ has a flatter distribution, but the plateau can still be recognized. These results of our *ab initio* MD simulations indicate that the helical chain structure persists in fluid Se even in the metallic state. On the other hand, Bichara *et al* [14] concluded, on the basis of the dihedral-angle distribution function obtained from their tight-binding MC simulation, that the structure of liquid Se does not contain helical chains. We consider that this discrepancy is caused by the fact that their method is not *ab initio* and includes some empirical parameters.

3.4. Bond breaking and rearrangement of Se chains

As stated in section 1, it has been determined experimentally that the average chain length decreases rapidly with increases in the temperature and pressure, and approaches a value of only about ten atoms in the metallic region [4]. Figure 8 shows the chain-length distribution function $L(N)$, with N being the number of atoms per chain, obtained from the present calculations. It is clearly shown in this figure that, at 870 K, $L(N)$ is distributed over a wide range of N, while, at 1770 K, $L(N)$ is distributed mainly over small $N < 10$. This temperature dependence of $L(N)$ is in agreement with the experimentally observed tendency. By investigating the time change of the chain structure, it is found that the interaction between the Se chains is important for bond breaking and rearrangement of the Se chains. When a Se chain moves in very close to one of the other chains, more than two

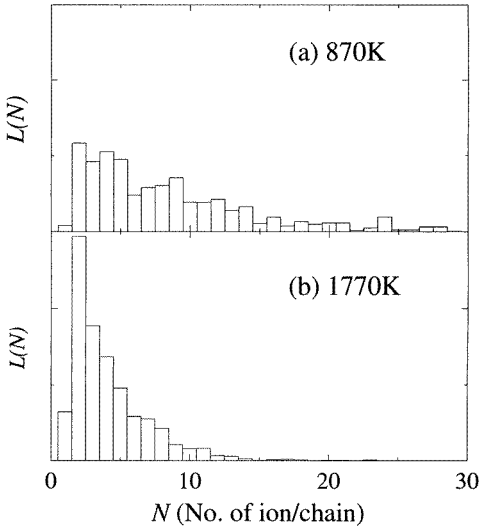

Figure 8. The chain-length distribution function $L(N)$, with N being the number of atoms per chain, for fluid Se calculated at (a) 870 K and (b) 1770 K.

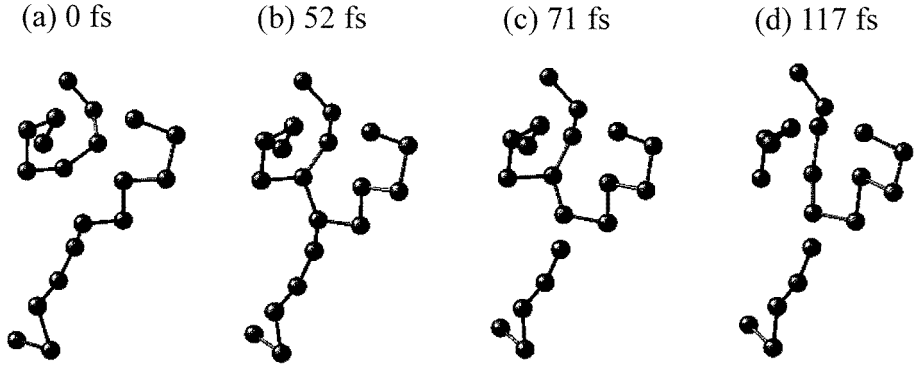

Figure 9. The time evolution of the local chain structure which is a part of the atomic configuration obtained by means of the MD simulation at 1770 K. Two Se atoms, whose distance apart is smaller than 2.7 Å, are connected by the bond.

Se atoms interact with each other, i.e. threefold coordinations are formed transiently. Since such threefold coordinations are unstable, bond breaking and rearrangement of the Se chains occur, and as a result twofold-coordinated chains are formed. As a typical example of bond breaking and rearrangement of the Se chains, we show in figure 9 the time evolution of the local chain structure which is a part of the atomic configuration obtained from the MD simulation at 1770 K. In the figure, two Se atoms, whose distance apart is smaller than 2.7 Å, are connected by the bond. At 0 fs (figure 9(a)), the closest distance between the two Se chains is about 3.4 Å, and, therefore, the two Se chains are considered to be well separated. However, these two chains approach each other in a short time, and at 52 fs a new bond is formed between them with threefold coordinations as shown in figure 9(b). It is seen, from figure 9(c), that a Se atom is detached from the threefold-coordinated Se atom

at 71 fs. At 117 fs (figure 9(d)), bond breaking occurs again, and finally three chains are formed without threefold coordination. From such a careful and detailed investigation of the time change of the chain structure, we can see that bond breaking and rearrangement of the Se chains take place almost always with the interaction between the Se chains, and that bond breaking in a single chain with no interaction with other chains hardly occurs. The probability that a Se chain contacts another chain becomes high due to the thermal motion of the atoms with increasing temperature. As a result, at high temperatures, bond breaking occurs frequently, and the average chain length decreases as shown in figure 8.

3.5. The mechanism of the semiconductor–metal transition

As described in section 3.1, we succeeded in reproducing the SC–M transition in fluid Se with our *ab initio* MD simulations. Here, we consider the mechanism of the SC–M transition. As discussed in sections 3.2 and 3.3, the helical chain structure persists in fluid Se even in the metallic state. However, the average chain length decreases with increasing temperature as shown in figure 8. In addition, the first-neighbour intrachain PDF becomes lower, and the interchain PDF becomes higher at the position of the first minimum of $g(r)$ as shown in figure 5. It should be noted again that the electronic states below the E_F show p-like bonding or non-bonding character, and that those above E_F show p-like anti-bonding character. Recently, we have investigated the microscopic mechanism of bond breaking in the S_8 ring by means of an *ab initio* molecular-dynamics simulation [33], and it was found that if bond breaking occurs, the anti-bonding states are stabilized, while the bonding or non-bonding states become unstable. In the case of Se chains, we can expect similar phenomena. If a chain is cut and the distance between the two Se atoms increases, the electronic states which have bonding or non-bonding character become unstable, while the electronic states which have anti-bonding character become stable. The structural changes described above indicate that such a situation occurs in fluid Se at high temperatures. It is considered that this is one of the elemental processes of the SC–M transition in fluid Se.

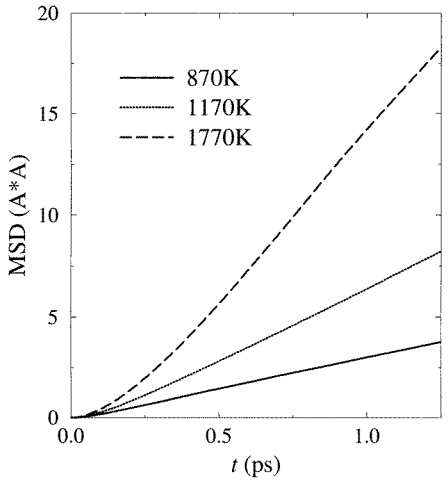

Figure 10. Mean square displacements at 870 K (solid line), 1170 K (dotted line), and 1770 K (dashed line) in units of Å^2.

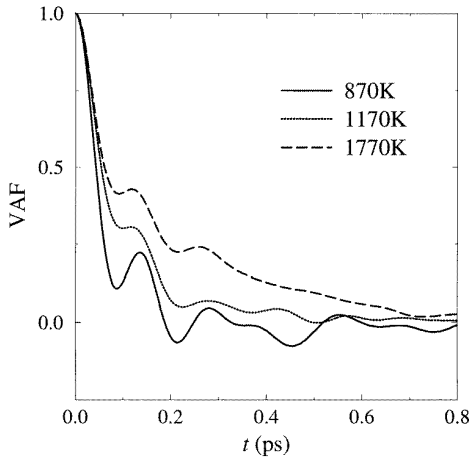

Figure 11. Normalized velocity autocorrelation functions at 870 K (solid line), 1170 K (dotted line), and 1770 K (dashed line).

3.6. Dynamic properties of atoms

It is interesting to investigate the dynamic properties of fluid Se in connection with the structural change discussed in section 3.2. We calculate the mean square displacement (MSD) and the velocity autocorrelation function (VAF), and these are shown in figures 10 and 11, respectively. It is seen, from figure 10, that the slope of the MSD becomes large with increasing temperature. The self-diffusion coefficients obtained from the MSD are 5.1, 11.9, and 25.1×10^{-5} cm^2 s^{-1} at 870, 1170, and 1770 K, respectively. These values are typical of liquid metals. This fact means that there is a high probability of a rapid rearrangement of the Se chains, especially in the metallic state. As shown in figure 9, such a rapid rearrangement is in fact confirmed by investigating the changes over time of the simulated chain structures. We can see, from figure 11, that the VAF has an oscillating behaviour at any temperature, though it decreases more slowly at higher temperatures reflecting the large diffusivity of Se atoms. The oscillating motion corresponds to the stretching vibration of Se–Se bonds. The frequency of the stretching vibration is found from the Fourier transform of the VAF to be about 220 cm^{-1}, which should be compared with the experimental values: about 250 cm^{-1} for amorphous and supercooled-liquid Se [34], and 237 cm^{-1} for trigonal Se [1]. It is very interesting that, at 1770 K, the stretching motion of Se–Se bonds persists in spite of the large amount of diffusion shown in figure 10.

4. Summary

In this paper, we have detailed our investigations into the semiconductor–metal (SC–M) transition in fluid Se using an *ab initio* molecular-dynamics simulation. We have used a cubic supercell containing 81 Se atoms with periodic boundary conditions. Three simulations have been carried out at different temperatures and densities: (870 K, 0.0286 Å^{-3}), (1170 K, 0.0270 Å^{-3}), and (1770 K, 0.0254 Å^{-3}). The states at two temperatures, 870 and 1170 K, are in the semiconducting region, while the state at 1770 K is in the metallic region. By investigating the temperature dependence of the electronic density of states, it has been confirmed that the SC–M transition in fluid Se is reproduced successfully by our MD simulations. To examine how structural changes occur with the SC–M transition in fluid Se, we have investigated the static properties of atoms, including the pair distribution function, the bond-angle and the dihedral-angle distribution functions, and the chain-length distribution function. It has been found that the chain-like structure persists even in the metallic state, though the chain structure is substantially disrupted. With increasing temperature, the average nearest-neighbour distance becomes a little shorter, the coordination number decreases slightly, and the average chain length decreases, in agreement with the experimentally observed tendency. By investigating the time changes of the chain structure, it has been found that the interaction between the Se chains is crucially important for bond breaking, and that bond breaking and rearrangement of the Se chains occur more frequently at higher temperatures. We have also investigated the dynamic properties of atoms. The self-diffusion coefficients have been found from the mean square displacements to be 5.1, 11.9, and 25.1×10^{-5} cm^2 s^{-1} at 870, 1170, and 1770 K, respectively, which are typical values for liquid metals. It has been found, from the velocity autocorrelation function, that, in the metallic state, the stretching motion of Se–Se bonds persists in spite of the large amount of diffusion. There has been some discussion on the microscopic mechanism of the SC–M transition. It is important to note that when the Se–Se bonds break, the anti-bonding states above the Fermi level (E_F) are stabilized while the bonding or non-

bonding states below E_F become unstable, and, therefore, the gap at E_F disappears at high temperatures.

Acknowledgments

This work was supported by a Grant-in-Aid for Scientific Research on Priority Areas (No 07236102) from the Ministry of Education, Science, Sports and Culture, Japan. We are grateful to Professor K Tamura, Professor M Inui, and Dr Y Sakaguchi for useful discussions. The authors thank the Supercomputer Centre, Institute for Solid State Physics, University of Tokyo, for the use of the FACOM VPP500.

References

[1] Gerlach E and Grosse P 1979 *The Physics of Selenium and Tellurium; Proc. Int. Conf. on the Physics of Selenium and Tellurium (Königstein, Germany, 1979)* (Berlin: Springer)
[2] Perron J C, Rabit J and Rialland J F 1982 *Phil. Mag.* B **46** 321
[3] Freyland W and Cutler M 1980 *J. Chem. Soc. Faraday Trans.* **76** 756
[4] Warren W W Jr and Dupree R 1980 *Phys. Rev.* B **22** 2257
[5] Hoshino H, Schmutzler R W and Hensel F 1976 *Ber. Bunsenges. Phys. Chem.* **80** 27
[6] Hoshino H, Schmutzler R W, Warren W W Jr and Hensel F 1976 *Phil. Mag.* B **33** 255
[7] Edeling M and Freyland W 1981 *Ber. Bunsenges. Phys. Chem.* **85** 1049
[8] Tamura K and Hosokawa S 1992 *Ber. Bunsenges. Phys. Chem.* **96** 681
[9] Tamura K 1996 *J. Non-Cryst. Solids* **205–207** 239
[10] Inui M, Noda T and Tamura K 1996 *J. Non-Cryst. Solids* **205–207** 261
[11] Endo H 1983 *J. Non-Cryst. Solids* **59+60** 1047
[12] Hohl D and Jones R O 1991 *Phys. Rev.* B **43** 3856
[13] Almarza N G, Enciso E and Bermejo F J 1993 *J. Chem. Phys.* **99** 6876
[14] Bichara C, Pellegatti A and Gaspard J-P 1994 *Phys. Rev.* B **49** 6581
[15] Kirchhoff F, Gillan M J and Holender J M 1996 *J. Non-Cryst. Solids* **205–207** 924
[16] Kirchhoff F, Gillan M J, Holender J M, Kresse G and Hafner J 1996 *J. Phys.: Condens. Matter* **8** 9353
[17] Vanderbilt D and Joannopoulos J D 1983 *Phys. Rev.* B **27** 6296
Vanderbilt D and Joannopoulos J D 1983 *Phys. Rev.* B **27** 6302
[18] Hamilton K G 1986 *Phys. Rev.* B **34** 5708
[19] Zhong H, Levine Z H, Allan D C and Wilkins F W 1992 *Phys. Rev. Lett.* **69** 379
[20] Robertson J 1976 *Phil. Mag.* B **34** 13
[21] Vanderbilt D and Joannopoulos J D 1979 *Phys. Rev. Lett.* **42** 1012
Vanderbilt D and Joannopoulos J D 1983 *Phys. Rev.* B **27** 6311
[22] Li Z Q, Yu J Z, Ohno K, Gu B L, Czajka R, Kasuya A, Nishina Y and Kawazoe Y 1995 *Phys. Rev.* B **52** 1524
[23] Springborg M and Jones R O 1988 *J. Chem. Phys.* **88** 2652
[24] Ikawa A and Fukutome H 1989 *J. Phys. Soc. Japan* **58** 4517
[25] Perdew J P 1991 *Electronic Structure of Solids '91* ed P Ziesche and H Eschrig (Berlin: Akademie)
[26] Teter M P, Payne M C and Allan D C 1989 *Phys. Rev.* B **40** 12 255
[27] Kresse G and Hafner J 1994 *Phys. Rev.* B **49** 14 251
[28] Shimojo F, Zempo Y, Hoshino K and Watabe M 1995 *Phys. Rev.* B **52** 9320
[29] Vanderbilt D 1990 *Phys. Rev.* B **41** 7892
[30] Nosé S 1984 *Mol. Phys.* **52** 255
[31] Hoover W G 1985 *Phys. Rev.* A **31** 1695
[32] Arias T A, Payne M C and Joannopoulos J D 1992 *Phys. Rev.* B **45** 1538
[33] Shimojo F, Hoshino K and Zempo Y 1998 *J. Phys.: Condens. Matter* submitted
[34] Carroll P J and Lannin J S 1980 *J. Non-Cryst. Solids* **35+36** 1277